


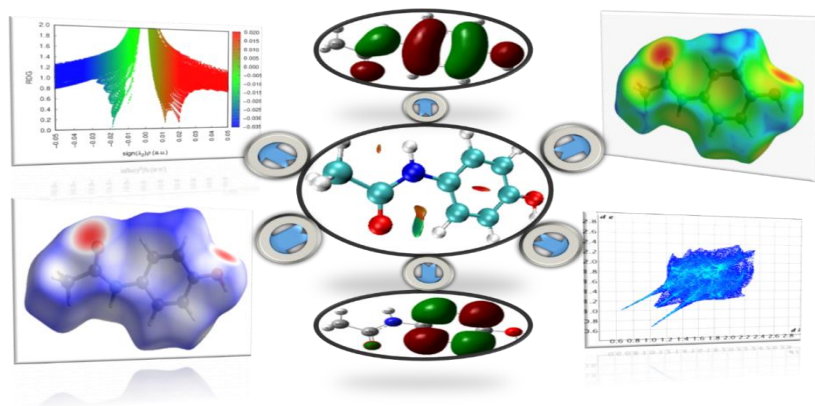
Full Paper | <http://dx.doi.org/10.17807/orbital.v17i1.19889>

# A Comprehensive Study of Pharmacologic Complexity: Study of Interactions and Properties of Paracetamol, Aspirin, Naproxen, and Diclofenac

Yousif H. Azeez <sup>a</sup>, Rebaz A. Omer <sup>b,c</sup>, Khdir A. Othman <sup>b</sup>, Karzan A. Omar <sup>b</sup>, Aryan F. Qader\* <sup>b</sup>

The present study explores the molecular and electronic properties of four widely used pharmaceutical compounds—Paracetamol, Aspirin, Naproxen, and Diclofenac—to enhance our understanding of their stability, reactivity, and potential applications in drug design. Through computational analysis, key electronic properties and intermolecular interactions were examined to reveal factors influencing their chemical behavior. Using density functional theory (DFT) with the B3LYP/6-31G(d,p) level, the study investigates their electronic structure, charge distribution, and optical characteristics. Reduced Density Gradient (RDG) and Non-Covalent Interaction (NCI) analyses highlight distinct intermolecular interactions, such as strong hydrogen bonding in Paracetamol,  $\pi \rightarrow \pi^*$  transition stabilization in Aspirin, dispersion interactions in Naproxen, and diverse attractive forces in Diclofenac. Natural Bond Orbital (NBO) analysis further elucidates electron delocalization effects. The study also evaluates Nonlinear Optical (NLO) properties, suggesting potential applications beyond pharmaceuticals. Quantum chemical parameters indicate that Aspirin has the highest ionization energy (10.18 eV), making it a strong electron acceptor, while Paracetamol demonstrates significant electron-donating ability. Molecular Electrostatic Potential (MEP) mapping provides insights into charge distribution and reactivity, while UV-Visible absorption spectra reveal optical characteristics relevant to various applications. These findings offer valuable insights into the fundamental electronic behavior of these pharmaceutical compounds, which may inform drug formulation, bioavailability studies, and potential modifications for enhanced therapeutic efficacy. By linking computational analysis with pharmaceutical applications, this study contributes to a deeper understanding of molecular interactions that govern drug stability and performance.

## Graphical abstract



## Keywords

Drug likeness  
Molecular reactivity  
Materials science  
NCI methodologies  
Pharmaceutical molecules  
Quantum electronic properties

## Article history

Received 16 Dec 2023  
Revised 14 Mar 2025  
Accepted day 14 Apr 2025  
Available online 27 Apr 2025

Handling Editor: Adilson Beatriz

<sup>a</sup> University of Halabja, College of Science, Department of Physics, Halabja, Iraq. <sup>b</sup> Department of Chemistry, Faculty of Science and Health, Koya University, Koya KOY45, Kurdistan Region - F.R. Iraq. <sup>c</sup> Department of Pharmacy, College of Pharmacy, Knowledge University, Erbil 44001, Iraq. \*Corresponding author. E-mail: [aryan.qader@koyauniversity.org](mailto:aryan.qader@koyauniversity.org)

## 1. Introduction

Pharmaceutical research hinges on an in-depth understanding of drug compounds and their molecular properties, as such insights are crucial for rational drug design and therapeutic advancements. In this study, we investigate four widely used nonsteroidal anti-inflammatory drugs (NSAIDs)—Paracetamol, Aspirin, Naproxen, and Diclofenac—due to their broad clinical applications in pain relief, inflammation reduction, and fever management [1-4]. These drugs were selected based on their established pharmacological significance and widespread use in global healthcare systems. Understanding their molecular interactions, electronic properties, and structural behavior can contribute to optimizing their therapeutic efficacy and guiding the development of improved pharmaceutical agents [5, 6].

Assumes a central role, facilitating the visualization and systematic characterization of molecular packing arrangements. The utilization of parameters such as  $d_i$ ,  $d_e$ ,  $d_{norm}$ , shape index, curvedness, and relative contributions to the percentage of the Hirschfeld surface area delves into the intricacies of intermolecular contacts, unveiling a comprehensive spatial understanding of the studied compounds [7]. In augmenting this analysis, a foray into drug likeness entails an evaluation of Molinspiration property values against standard drug molecules [8, 9]. Integrating natural bond orbital structure (NBO) analysis and Second Order Perturbation Theory Analysis of the Fock Matrix in NBO enrich our comprehension of the electronic structure and bonding patterns within the compounds [10, 11]. Delving further, a study of nonlinear optical properties (NLO) uncovers the distinctive behavior of the title compound across diverse phases. The scrutiny of Frontier molecular orbitals and an array of quantum chemical parameters—embracing HOMO and LUMO energies, ionization energy, electron affinity, energy gap, hardness, softness, electronegativity, chemical potential, electrophilicity, nucleophilicity, back-donation, and electron transfer—demystifies the electronic intricacies and reactivity profiles of the compounds [12-16]. The analysis includes total energy, molecular electrostatic potential (MEP) maps, and theoretical UV-Vis absorption spectra, providing a thorough depiction of the compounds' energetic profiles and spectroscopic properties [17, 18]. By harmonizing these advanced techniques, this research unveils a comprehensive perspective of the molecular properties, interactions, and potential applications of paracetamol, Aspirin, Naproxen, and diclofenac [19-23]. This study offers a comprehensive exploration of Paracetamol, Aspirin, Naproxen, and Diclofenac through diverse analytical techniques. The findings deepen our understanding of intermolecular interactions, electronic properties, charge distribution, and optical characteristics, while also highlighting potential applications of these pharmaceutical compounds. Ultimately, these insights contribute to more informed drug design and development, driving progress in pharmaceutical research and therapeutic advancements.

## 2. Results and Discussion

### 2.1. Reduced density gradient (RDG) and Non-covalent interaction (NCI)

Reduced density gradient (RDG) and non-covalent interactions (NCI) studies are novel methodologies used for the characterization of weak intermolecular interactions. The NCI index is used for characterizing intermolecular

interactions and evaluating the characteristics of weak interactions. The NCI index is derived from the reduced density gradient (RDG) and offers further support for non-covalent interactions. The reduced density gradient (RDG) is a fundamental dimensionless parameter that encompasses the density and its initial derivative, as denoted by the following equation [24-26].

$$RDG(r) = \frac{1|\nabla\rho(r)|}{2(3\pi r^2)^{\frac{1}{3}}\rho^{\frac{4}{3}}(r)}$$

The colored RDG scatter plots were generated using the Multiwfn software, while the 3D isosurface was shown using the VMD software [27]. The NCI studies were conducted using an isosurface threshold of 0.5. The isosurface range for the RDG is from -0.035 to 0.02 atomic units. Fig. 1 exhibits the 2D RDG plots and the 3D isosurface.

The determination of the nature and strength of interactions within a molecule is facilitated by plotting the function  $\rho(r)$  against the sign of  $\lambda_2$ . Specifically, the value of  $\text{sign}(\lambda_2)$  plays a crucial role in this prediction. When  $\text{sign}(\lambda_2) \rho < 0$ , it shows an attractive interaction (bonded). Conversely, when  $\text{sign}(\lambda_2) \rho > 0$ , it signifies a repulsive interaction (non-bonded).

The RDG scatter graphs show many spikes, as seen in Fig. 1. The spikes are categorized into three distinct areas based on the values of  $\text{sign}(\lambda_2) \rho$ . The various zones are distinguished by their colors, including red, green, and blue. The blue area in the diagram represents strong attractive contacts, including strong hydrogen bonds. The green region may be characterized as weak attractive interactions, known as van der Waals forces. The red region shows strong repulsive interactions, which are attributed to the steric effect [28]. In diclofenac, the dots on the graph are more densely packed than with other compounds; this suggests that the weak hydrogen bonds and van der Waals interactions are more powerful. As well as, according to the NCI-RDG scatter plots, the red regions can be found inside the aromatic rings, showing a steric effect caused by strong repulsions. The green-colored isosurface, which attributes to vdW interactions, lies between the oxygen atom and the hydrogen atom (O-H), showing weak H-bond interaction and other interactions between the two hydrogen atoms (H-H).

Moreover, van der Waals interactions (depicted in green in the RDG isosurface) contribute to molecular recognition and binding affinity between the drug and its biological target. The relatively dense distribution of weak hydrogen bonds and van der Waals forces in diclofenac, as observed in our RDG scatter plots, suggests enhanced molecular stability in the binding pocket of target proteins. This, in turn, can influence drug efficacy and selectivity. Additionally, steric effects (highlighted in the red regions of the RDG scatter plots) can impact drug metabolism by affecting the accessibility of metabolic enzymes. For example, steric hindrance around aromatic rings may slow enzymatic oxidation, altering drug clearance rates and half-life. By considering these factors, our analysis provides insight into how non-covalent interactions influence the pharmacokinetic and pharmacodynamic properties of the studied compounds. We have incorporated these points into the revised manuscript to better align with the reviewer's concerns.

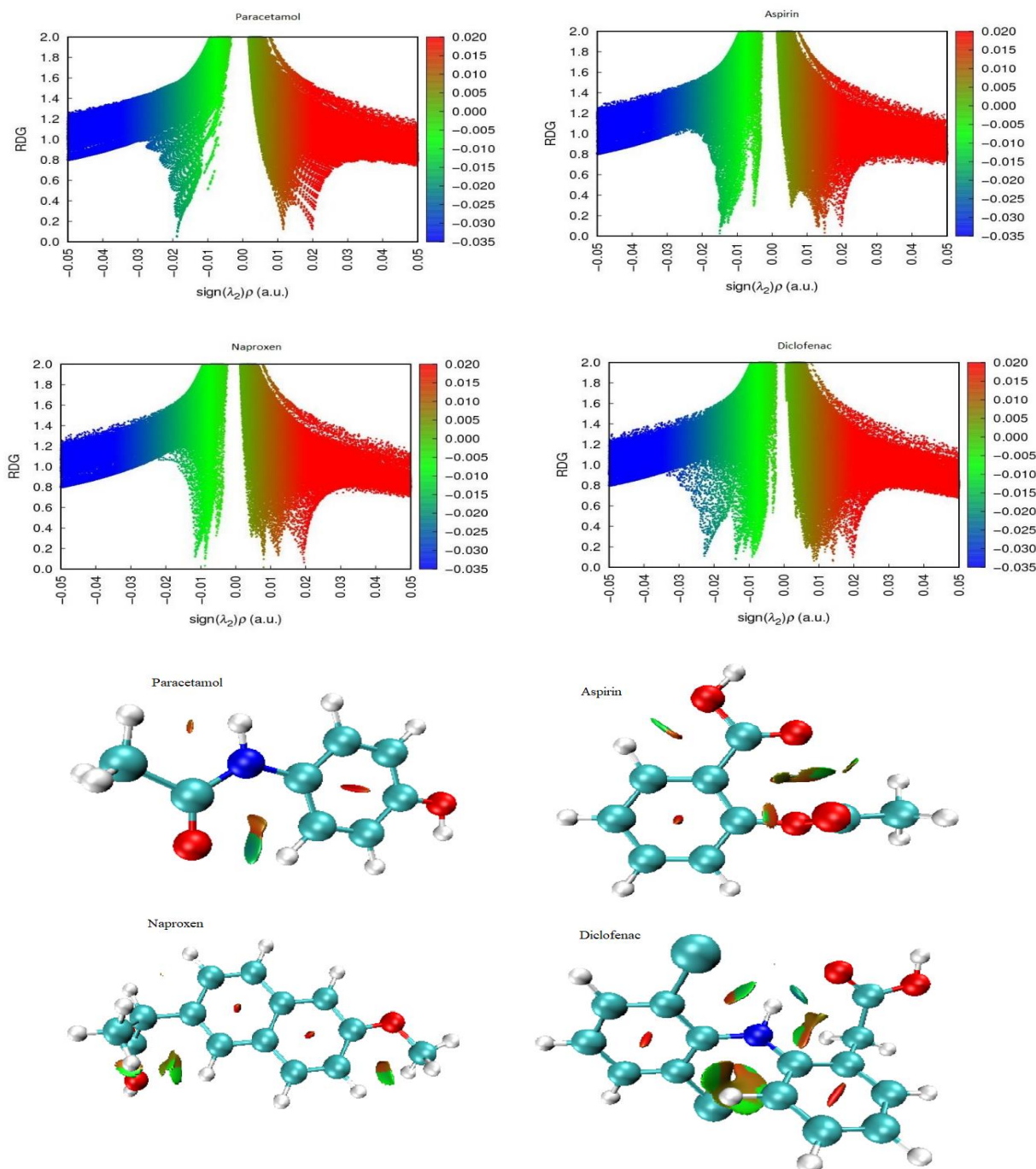


Fig. 1. Reduced Density Gradient (RDG) analysis showing weak and strong interaction of all compounds.

## 2.2. Hirschfeld Analysis

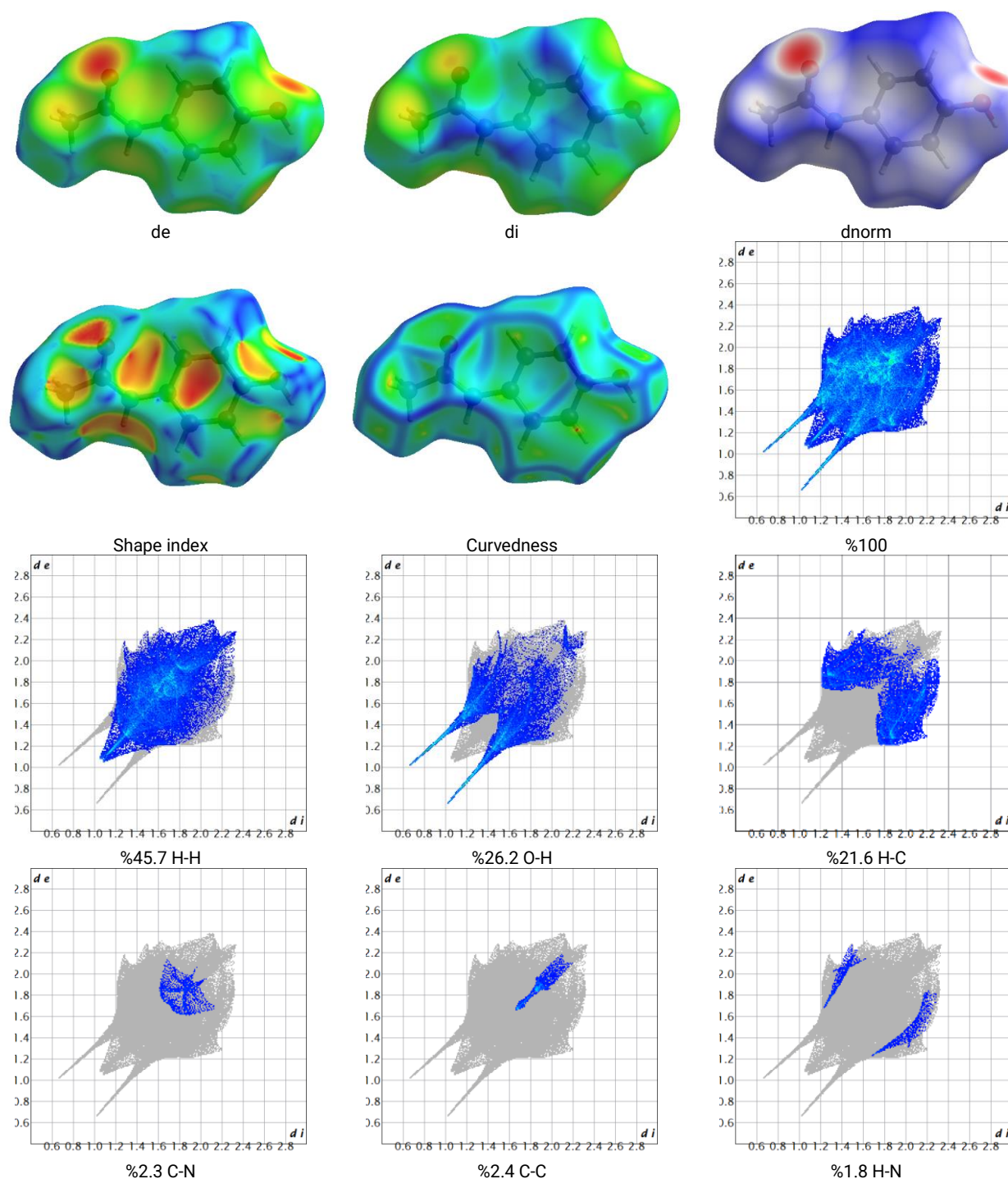
The Hirschfeld surface technique is a distinctive approach used to comprehend intermolecular interactions and get insights into patterns seen in crystal packing. The present investigation was conducted to examine the existence of hydrogen bonds and other types of weak intermolecular interactions inside the crystal structure [29, 30]. The Hirschfeld surface mapped over  $d_{\text{norm}}$  and 2D fingerprint plots (FPs) were produced using Crystal Explorer 17.5 software [31]. The intermolecular interactions are described by the use of Hirschfeld analysis, which employs a color-coded representation consisting of red, blue, and white. The red areas, characterized by negative  $d_{\text{norm}}$  values, show distances less than the van der Waals (vdW) radius.

Conversely, the dark blue color corresponds to positive  $d_{\text{norm}}$  values, indicating contacts longer than the vdW radii. The white regions represent contacts equal to the van der Waals radii, with a  $d_{\text{norm}}$  value of 0. The Hirschfeld surface displayed on  $d_{\text{norm}}$  (circled deep-red and smaller spots reflect intermolecular hydrogen bonds). The shape index and curvedness of the Hirschfeld surface a valuable tool used for the identification of C-H $\cdots$  $\pi$  and  $\pi$ - $\pi$  stacking interactions [32]. These interactions can be recognized by adjacent red and blue triangles. Conversely, the absence of neighboring red and/or blue triangles shows the absence of  $\pi$ - $\pi$  interactions. The fingerprint traces have a blue-green color during these interactions. The two-dimensional FP plots provide insights on intermolecular interactions between atoms inside a system

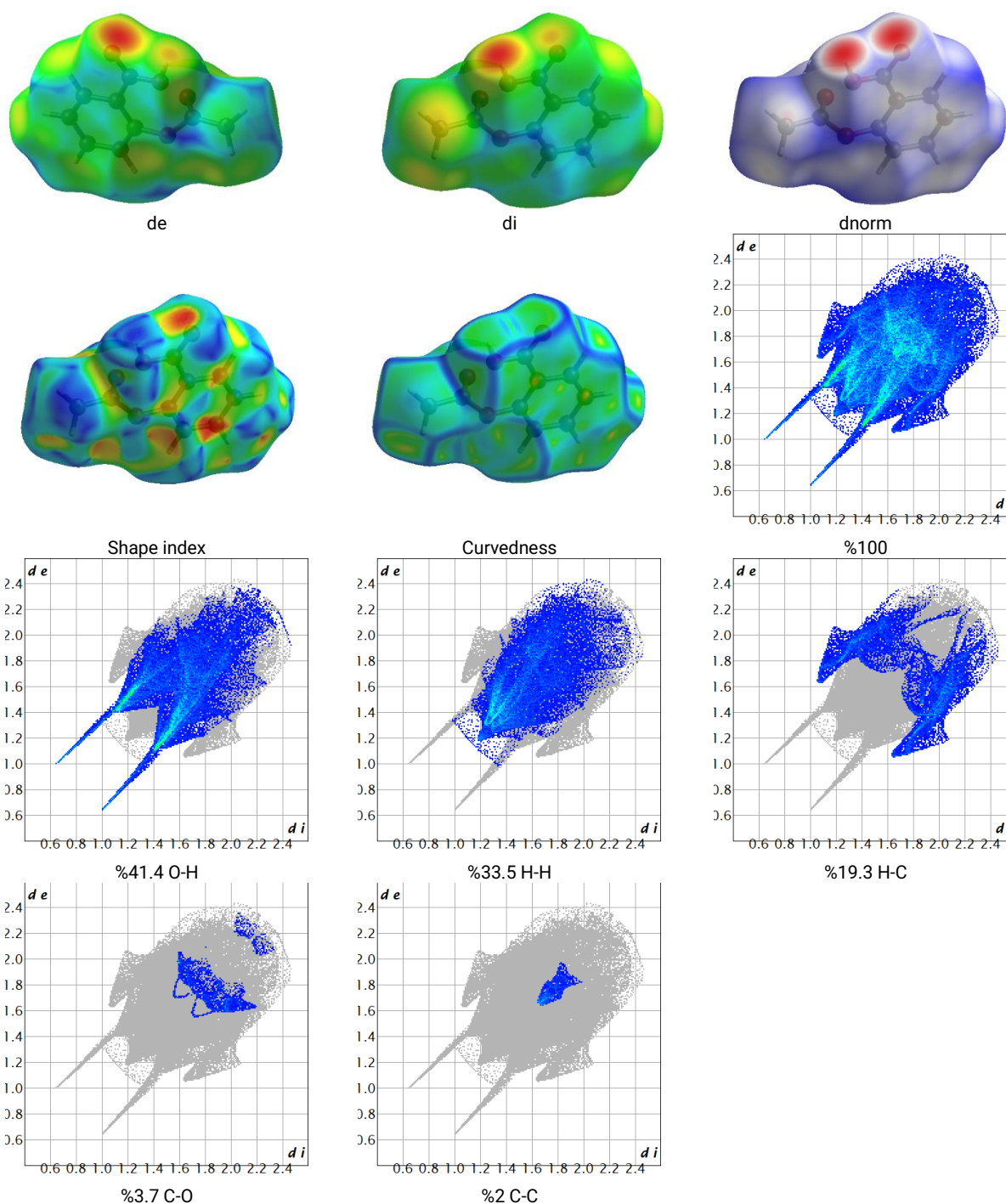


and atoms outside the system. These plots allow for the determination of the relative contribution of each kind of interaction to the overall surface area of the Hirshfeld surface. Hirshfeld surface, which is used to visualize the distribution of electron density, specifically highlighting intermolecular hydrogen bonding (IHB) in all compounds. The mapping presented highlights areas in bright red, indicating C $\cdots$ H $\cdots$ O/O $\cdots$ H contacts, which are associated with hydrogen bonding (IHB). In the paracetamol molecule, H $\cdots$ H interactions are the primary contributors, making up 45.7% of the total Hirshfeld surface, as depicted in Fig. 2. In contrast, for aspirin, as shown in Fig. 3, these interactions appear as dispersed

spots in the center of the two-dimensional fingerprint (2D FP) plot. Regarding molecular interactions, including C $\cdots$ H $\cdots$  $\pi$  and  $\pi\cdots\pi$  interactions, the C $\cdots$ H contacts are represented by two prominent symmetric wings on the upper and lower sides of the FP pattern. These C $\cdots$ H interactions significantly contribute to the overall Hirshfeld surface, accounting for approximately 30.5% of the surface area in the naproxen compound, as illustrated in Fig. 4. Additionally, the triangular C $\cdots$ C connections in the diclofenac compound are shown in blue-green within the central region of the FP plot, contributing 4.4%, as represented in Fig. 5.



**Fig. 2.** di, de, dnorm, shape index, curvedness, and relative contributions to the percentage of Hirshfeld surface area for the various intermolecular contacts in paracetamol.



**Fig. 3.** di, de, dnorm, shape index, curvedness, and relative contributions to the percentage of Hirshfeld surface area for the various intermolecular contacts in Aspirin.

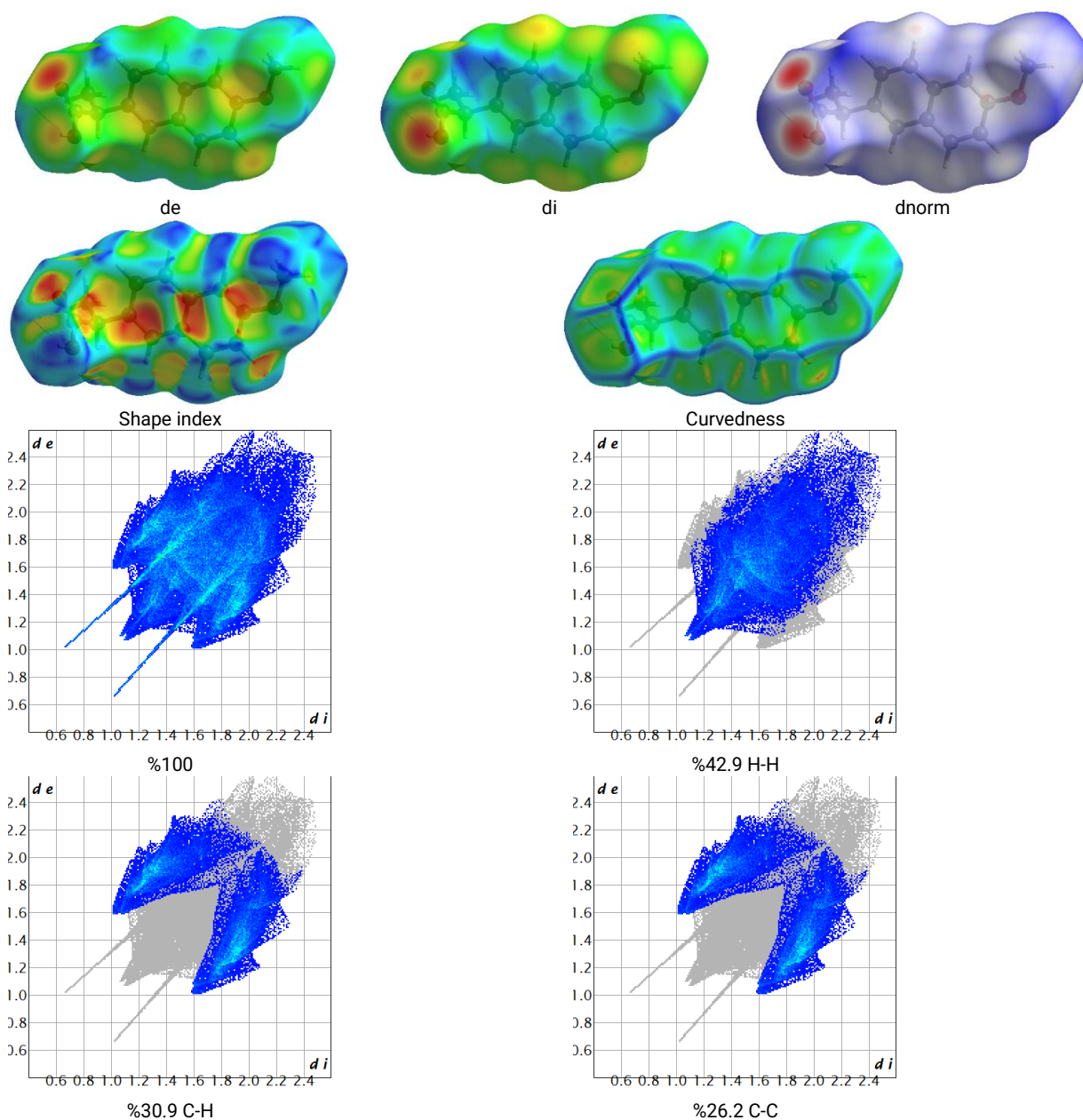
### 2.3. Drug likeness

The quantitative analysis of drug likeness properties [33, 34] has unveiled crucial insights into the pharmacological potential of Paracetamol, Aspirin, Naproxen, and Diclofenac. Exploring descriptors, including hydrogen bond donors (HBD), hydrogen bond acceptors (HBA), miLogP, polar surface area (PSA), molecular weight, and rotatable bonds, has offered a comparative understanding of their profiles. Paracetamol's low HBD (2) and HBA (3) values suggest limited polarity, potentially affecting its solubility and interactions. In contrast, Aspirin's higher HBD (1) and HBA (4) show a stronger hydrogen bonding capacity, aligned with its multifaceted therapeutic roles see Table 1. Diclofenac's elevated miLogP (4.57) highlights its lipophilic nature, while

Aspirin and Diclofenac's higher PSA values (63.60 and 49.33 Å<sup>2</sup>) emphasize their increased surface areas for interactions. The molecular weight of Diclofenac (296.15 g/mol) exceeds the others, influencing its bioavailability and metabolism. Paracetamol's lower molecular weight (151.16 g/mol) hints at enhanced diffusion across barriers. Rotatable bonds further distinguish the compounds, with Paracetamol (1), Aspirin (3), Naproxen (3), and Diclofenac (4) showcasing distinct molecular flexibilities. Understanding these properties is pivotal for rational drug design, guiding compound modification for specific therapeutic objectives and addressing potential limitations. These insights offer a roadmap for optimizing bioavailability, interactions, and minimizing challenges. By

leveraging these quantitative descriptors, researchers navigate drug design complexities, forging a path toward

targeted and effective pharmaceutical innovations.



**Fig. 4.** di, de, dnorm, shape index, curvedness, and relative contributions to the percentage of Hirshfeld surface area for the various intermolecular contacts in Naproxen.

**Table 1.** Molinspiration property values of study compounds and standard drug molecule.

Descriptors	Paracetamol	Aspirin	Naproxen	Diclofenac	Expected range
Hydrogen bond donor (HBD)	2	1	1	2	< 5
Hydrogen bond acceptors (HBA)	3	4	3	3	< 10
miLogP	0.68	1.43	3.38	4.57	< 5
Polar surface area (PSA) Å <sup>2</sup>	49.33	63.60	46.53	49.33	< 140
Molecular weight	151.16	180.16	230.26	296.15	< 500
Number of rotatable bonds	1	3	3	4	< 10



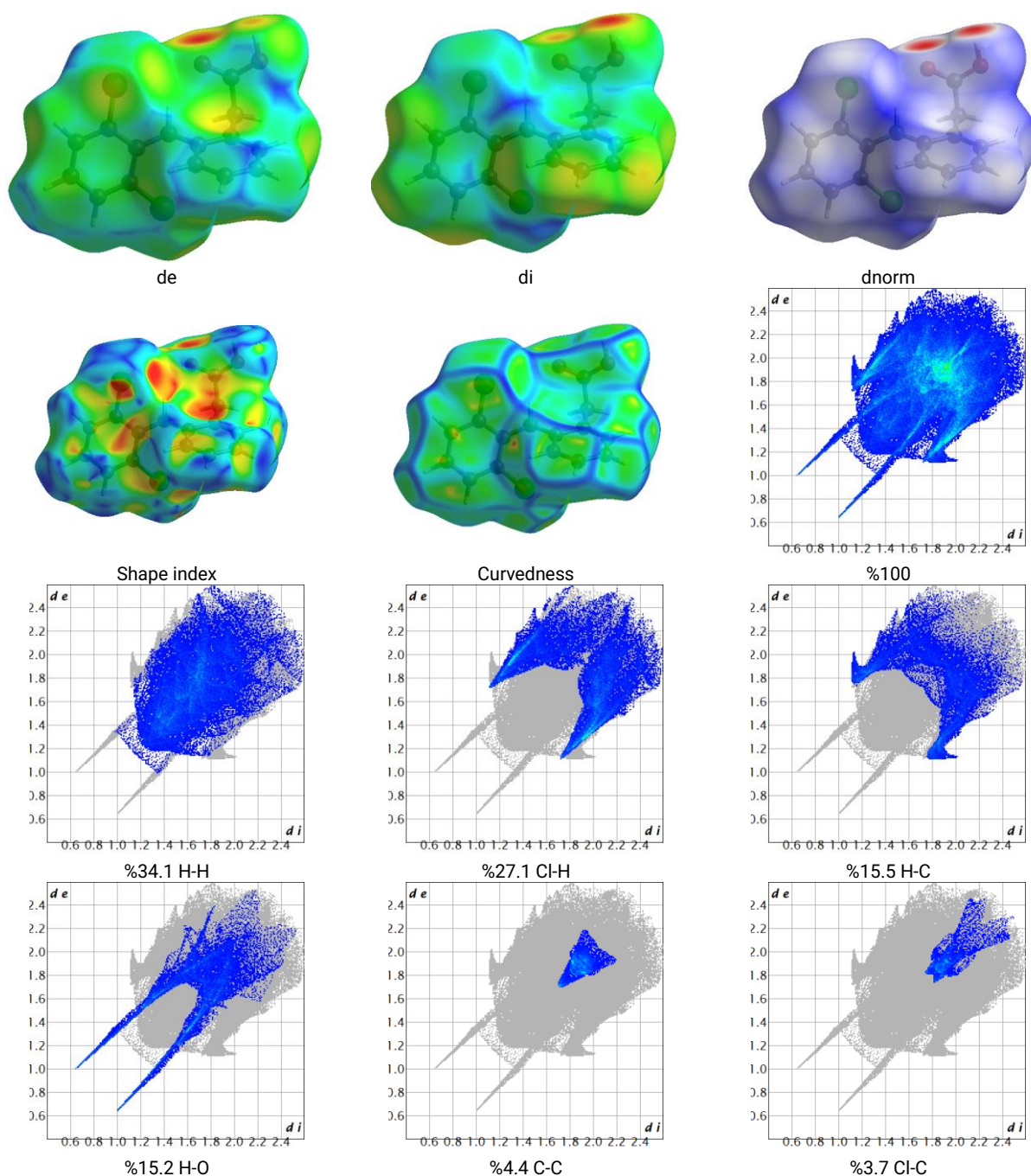


Fig. 5. di, de, dnorm, shape index, curvedness, and relative contributions to the percentage of Hirshfeld surface area for the various intermolecular contacts in diclofenac.

#### 2.4. Natural Bond Orbital (NBO) Structure Analysis

An examination of the natural bond orbital structure of the compound under investigation was carried out. Using the B3LYP/6-31G(d, p) theoretical approaches, the purpose of this investigation was to get an understanding of the interactions that take place between the Lewis orbitals and the non-Lewis orbitals of the molecule. The NBO analysis was conducted at the same theoretical level as the optimized structures to illustrate the occurrences of intramolecular and intermolecular hydrogen bonding, as well as the dispersion of  $\pi$  electrons throughout the molecule. The second order energy is used to estimate the stabilization energy, which signifies the magnitude of the delocalization interactions, for every individual donor Natural Bond Orbital (NBO) (i), acceptor NBO (j), and the  $E(2)$  value connected with the electron delocalization between the donor and the acceptor [[35-39]].

$$E^{(2)}q = \Delta E_{ij} = q_i \frac{F(i,j)^2}{\epsilon_j - \epsilon_i}$$

Within the given context, the symbol "qi" is used to denote the occupation of the donor orbital. The characters " $\epsilon_j$ " and " $\epsilon_i$ " are used to symbolize the diagonal elements, while " $F(i,j)$ " denotes the diagonal NBO Fock matrix elements. The NBO analysis has been further refined to emphasize its relevance in illustrating intramolecular charge transfer (ICT) and hydrogen bonding effects. The discussion now explicitly connects the computed stabilization energies to the observed electronic effects within the molecule. Additionally, we have clarified the significance of  $\pi \rightarrow \pi^*$  and  $\sigma \rightarrow \sigma^*$  interactions in modulating the electronic structure, which directly impacts the molecular stability and potential bioactivity of the compound. Table 2 is a comprehensive summary of the

hypothetical intense interactions that include  $\pi^* \rightarrow \pi^*$  electrons. The investigation of Aspirin reveals the occurrence of a transition from the  $\pi^*$  C5-C6 orbital to the  $\pi^*$  C8-C10 orbital, which exhibits a significant stabilization energy of 271.87 kcal/mol when compared to other pharmaceutical compounds. The findings show that  $\sigma \rightarrow \sigma^*$  interactions have a lower delocalization energy compared to  $\pi \rightarrow \pi^*$  interactions. Consequently, the electron density connected with  $\sigma$  bonds

has a greater magnitude when compared to that of  $\pi$  bonds. The computed interaction energy for the resonance in the molecule are reported to be 45.93 kcal/mol. The observed energies may be attributed to the transfer of electrons from the lone pair LP(1)C10 of the electron-donating groups to the antibonding acceptor  $\pi^*$  orbital formed by the interaction between the  $\pi^*$ (C11-C12) carbons atoms.

**Table 2.** Second Order Perturbation Theory Analysis of Fock Matrix in NBO for all compounds.

Donor NBO (i)	Acceptor NBO (j)	E(2) kcal/mol	E(j)-E(i) a.u.	F(i,j) a.u.
<b>Paracetamol</b>				
$\sigma$ N 3 - H 14	$\sigma^*$ O 2 - C 10	4.72	1.26	0.069
$\sigma$ N 3 - H 14	$\sigma^*$ C 4 - C 5	4	1.24	0.063
$\pi$ C 4 - C 5	$\pi^*$ C 6 - C 8	21.33	0.28	0.069
$\pi$ C 4 - C 5	$\pi^*$ C 7 - C 9	18.73	0.28	0.065
$\pi$ C 6 - C 8	$\pi^*$ C 4 - C 5	17.7	0.29	0.066
$\pi$ C 6 - C 8	$\pi^*$ C 7 - C 9	19.86	0.28	0.069
$\sigma$ C 10 - C 11	BD*( 1) N 3 - C 4	4.44	1.06	0.061
$\sigma$ C 11 - H 17	$\pi^*$ O 2 - C 10	4.14	0.53	0.045
LP ( 2) O 1	$\pi^*$ C 7 - C 9	28.22	0.35	0.095
LP ( 1) N 3	$\pi^*$ O 2 - C 10	62.1	0.28	0.119
<b>Aspirin</b>				
$\sigma$ O 2 - H 21	$\sigma^*$ C 6 - C 11	4.93	1.17	0.069
$\pi^*$ C 5 - C 6	$\pi^*$ O 3 - C 11	21.69	0.27	0.07
$\pi^*$ C 7 - C 9	$\pi^*$ C 5 - C 6	24.42	0.28	0.074
$\pi^*$ C 7 - C 9	$\pi^*$ C 8 - C 10	17.52	0.29	0.064
$\sigma$ C 7 - H 14	$\sigma^*$ C 5 - C 6	4.68	1.08	0.064
$\sigma$ C 13 - H 20	$\pi^*$ O 4 - C 12	6.65	0.52	0.055
LP ( 2) O 2	$\pi^*$ O 3 - C 11	45.97	0.34	0.114
LP ( 2) O 3	$\sigma^*$ C 6 - C 11	18.81	0.69	0.104
$\pi^*$ O 3 - C 11	$\pi^*$ C 5 - C 6	172.79	0.01	0.076
$\pi^*$ C 5 - C 6	$\pi^*$ C 8 - C 10	271.87	0.01	0.08
<b>Naproxen</b>				
$\pi$ C 3 - C 4	$\pi^*$ C 11 - C 12	16.2	0.29	0.061
$\sigma$ C 4 - H 21	$\sigma^*$ C 3 - C 12	4.61	1.04	0.062
$\pi$ C 6 - C 7	$\pi^*$ C 8 - C 9	16.99	0.3	0.064
$\pi$ C 8 - C 9	LP ( 1) C 10	38.15	0.15	0.087
$\pi$ C 8 - C 9	$\pi^*$ C 6 - C 7	17.35	0.29	0.064
$\sigma$ C 9 - H 24	$\sigma^*$ C 7 - C 8	4.39	1.06	0.061
$\sigma$ O 17 - H 31	$\sigma^*$ C 13 - C 15	4.76	1.12	0.066
LP*( 1) C 5	$\pi^*$ C 3 - C 4	61.6	0.13	0.099
LP ( 1) C 10	$\pi^*$ C 8 - C 9	58.68	0.14	0.101
LP ( 1) C 10	$\pi^*$ C 11 - C 12	66.42	0.13	0.104
<b>Diclofenac</b>				
$\sigma$ O 3 - H 30	$\sigma^*$ C 8 - C 16	4.87	1.12	0.067
$\pi$ C 6 - C 10	$\pi^*$ C 7 - C 11	20.48	0.28	0.069
$\pi$ C 7 - C 11	$\pi^*$ C 12 - C 13	21.9	0.29	0.071
$\sigma$ C 8 - H 20	$\pi^*$ O 4 - C 16	4.69	0.51	0.046
$\sigma$ C 8 - H 21	$\sigma^*$ O 4 - C 16	4.95	1.09	0.066
$\pi^*$ C 12 - C 13	$\pi^*$ C 6 - C 10	22.09	0.28	0.071
LP ( 2) O 3	$\pi^*$ O 4 - C 16	48.61	0.34	0.116
LP ( 1) N 5	$\pi^*$ C 9 - C 15	22.72	0.26	0.073
$\pi^*$ C 9 - C 15	$\pi^*$ C 18 - C 19	137.96	0.02	0.08
$\pi^*$ C 14 - C 17	$\pi^*$ C 18 - C 19	224.25	0.01	0.084

## 2.5. Nonlinear optical properties (NLO):

Materials known as non-linear optical (NLO) play an important position in nonlinear optics. In particular, these materials have a significant influence on the fields of information technology and industrial applications. The geometry that had been optimized using B3LYP/6-31G+(d,p) was subjected to the first static analysis that was carried out. The initial static hyper-polarizability value, represented as ( $\beta_0$ ), is a tensor of three dimensions with a rank of three. It may be mathematically represented as a 3×3×3 matrix. The total static dipole moment ( $\mu_t$ ), mean polarizability ( $\alpha_0$ ), and initial static hyper-polarizability ( $\beta_0$ ) may be calculated using the equations that include the x, y, and z components [35, 40].

$$\begin{aligned}\mu_t &= [\mu_x^2 + \mu_y^2 + \mu_z^2]^{\frac{1}{2}} \\ \alpha_t &= (\alpha_{xx} + \alpha_{yy} + \alpha_{zz})/3 \\ \beta_t &= (\beta_x^2 + \beta_y^2 + \beta_z^2)^{1/2} \\ \beta_x &= \beta_{xxx} + \beta_{xyz} + \beta_{xzz} \\ \beta_y &= \beta_{yy} + \beta_{xyy} + \beta_{yzz} \\ \beta_z &= \beta_{zzz} + \beta_{xxz} + \beta_{yzz}\end{aligned}$$

A large magnitude of a certain component of the polarizability and hyper-polarizability suggests an important dispersion of charge in specific orientations [41, 42]. Table 3 and Table 4 presents the computed values for the total molecular dipole moment ( $\mu_t$ ), mean polarizability ( $\alpha_0$ ), and initial hyper-polarizability ( $\beta_0$ ) as mentioned in the title in



various solvents like water, DMSO, and methanol. The polarizabilities ( $\alpha_0$ ) and hyper-polarizabilities ( $\beta_0$ ) derived from the GAUSSIAN 09 output are first presented in atomic units (a.u.). In order to enhance comparability and comprehension, the aforementioned computed values have been transformed into units of electrostatic units (e.s.u.). The conversion factors used in this study are as follows: for polarizabilities ( $\alpha$ ), 1 atomic unit (a.u.) is equivalent to  $0.1482 \times 10^{-24}$  electrostatic units (e.s.u.), and for hyper-polarizabilities ( $\beta$ ), 1 a.u. is equivalent to  $8.6393 \times 10^{-33}$  e.s.u. As seen in Table 3 and Table 4, the computed dipole moment ( $\mu$ ) values for the investigated compound exceed the dipole moment of Urea ( $\mu=1.3732$  D). Urea is often used as a representative molecule for the examination of the nonlinear optical (NLO) characteristics of molecular systems. As a result, it has often

been used as a standard for conducting comparative analysis.

The polarizability values were determined for the gas phase and various solvents, including water, DMSO, and methanol. The values are shown in Table 3 and Table 4. The polarizability of paracetamol is greater in water when compared to other solvents, while diclofenac has the lowest polarizability in water. The determination of the size of ( $\beta_0$ ) has significant importance within the context of a nonlinear optical (NLO) system. The  $\beta_0$  values of all medications have a relatively reduced magnitude when compared to the ( $\beta_0$ ) value of urea, which is measured at  $343.272 \times 10^{-33}$  esu. Based on the aforementioned results, the investigated compounds might not have the potential for Nonlinear Optical (NLO) applications.

**Table 3.** Nonlinear optical properties for a title compound in gas phase and aqueous phases.

parameters	Paracetamol				Aspirin			
	Gas phase	water	DMSO	methanol	Gas phase	water	DMSO	methanol
$\mu_x$	0.2724	0.2846	0.2848	0.2850	-1.5118	-2.0745	-2.0663	-2.0574
$\mu_y$	2.0406	2.8297	2.8163	2.8019	-0.2057	-0.4434	-0.4383	-0.4330
$\mu_z$	-0.0005	-0.0006	-0.0006	-0.0006	-1.3182	-1.6246	-1.6192	-1.6134
$\mu_t$	2.0587	2.8440	2.8306	2.8164	2.0163	2.6720	2.6614	2.6502
$\alpha_{xx}$	-58.02	-56.94	-56.95	-56.96	-63.49	-60.88	-60.92	-60.97
$\alpha_{yy}$	-58.40	-57.33	-57.35	-57.37	-61.39	-59.41	-59.45	-59.48
$\alpha_{zz}$	-65.93	-65.9787	-65.9775	-65.9761	-79.16	-79.58	-79.57	-79.56
$\alpha_0$	-60.78	-60.08	-60.09	-60.10	-68.01	-66.62	-66.65	-66.67
$\alpha$ (esu) * $10^{-24}$	-9.01	-8.90	-8.91	-8.91	-10.08	-9.87	-9.88	-9.88
$\beta_{xxx}$	18.24	20.63	20.61	20.60	15.21	11.49	11.55	11.61
$\beta_{xyy}$	-23.28	-24.93	-24.91	-24.88	0.45	-1.84	-1.80	-1.77
$\beta_{xzz}$	5.52	5.75	5.75	5.75	2.58	1.75	1.76	1.77
$\beta_x$	0.48	1.45	1.45	1.46	18.25	11.40	11.51	11.62
$\beta_{yyy}$	5.19	9.12	9.06	8.99	35.90	36.15	36.16	36.17
$\beta_{xxy}$	-8.66	-5.74	-5.79	-5.85	-12.12	-16.38	-16.31	-16.23
$\beta_{yzz}$	-3.14	-2.78	-2.79	-2.80	9.46	9.43	9.43	9.43
$\beta_y$	-6.61	0.60	0.47	0.34	33.23	29.20	29.28	29.37
$\beta_{zzz}$	0.00	0.00	0.00	0.00	-4.78	-5.95	-5.93	-5.91
$\beta_{xxz}$	0.00	-0.01	-0.01	-0.01	-0.93	-2.17	-2.15	-2.13
$\beta_{yyz}$	0.00	0.00	0.00	0.00	-0.24	-0.76	-0.75	-0.74
$\beta_z$	0.00	-0.01	-0.01	-0.01	-5.95	-8.88	-8.83	-8.78
$\beta_0$ (esu) * $10^{-33}$	6.630	1.568	1.530	1.450	38.379	32.582	32.678	32.780

## 2.6. Frontier Molecular Orbitals and Quantum Chemical Parameters

Fig. 6 presents the HOMO and LUMO orbitals of the four drugs [43, 44]. With Paracetamol, the HOMO exhibits electron density predominantly around oxygen and nitrogen atoms, suggesting heightened reactivity, while the LUMO's electron density spans the entire molecule, implying its potential to accept electrons. Similarly, in Aspirin, the HOMO's electron density is concentrated around carboxylic acid and oxygen atoms, showing reactivity, while the LUMO displays widely distributed electron density, suggesting its capacity to receive electrons. Naproxen's HOMO shows electron density localized at oxygen and nitrogen atoms, signifying reactivity, and its LUMO shows an evenly dispersed electron density, showing its ability to accept electrons. In Diclofenac, the HOMO's electron density is mainly around chlorine and oxygen atoms, suggesting potential reactivity, and the LUMO's electron density spans the entire molecule, showcasing its capacity to receive electrons. In the quantum's investigation chemical parameters for the title compound and three pharmaceutical drugs, namely Paracetamol, Aspirin, Naproxen, and Diclofenac, several important electronic characteristics were examined and compared (Table 5). The HOMO (Highest

Occupied Molecular Orbital) and LUMO (Lowest Unoccupied Molecular Orbital) energies play a crucial role in understanding the reactivity and stability of molecules. Paracetamol exhibited the lowest HOMO energy (-5.482 eV), showing its higher electron-donating ability compared to the other drugs. Aspirin had the most negative LUMO energy (-1.485 eV), suggesting its strong electron-accepting behavior.

The ionization energy [[45]], representing the energy required to remove an electron from a neutral molecule, was highest for Aspirin (6.927 eV), followed by Paracetamol (5.482 eV), Naproxen (5.466 eV), and Diclofenac (5.553 eV). The electron affinity, showing the energy released when an electron is added to a neutral molecule, was the highest for Aspirin (1.485 eV). This suggests that aspirin has a greater tendency to accept electrons compared to the other compounds. The energy gap [46], calculated as the difference between the LUMO and HOMO energies, determines a molecule's stability and reactivity. Paracetamol exhibited the widest energy gap (5.490 eV), signifying its relatively higher stability among the studied compounds. The hardness values, representing the resistance to electron addition or removal, were comparable among the drugs, with Paracetamol and Aspirin showing similar values.

**Table 4.** Nonlinear optical properties for a title compound in gas phase.

parameters	naproxen				diclofenac			
	Gas phase	water	DMSO	methanol	Gas phase	water	DMSO	methanol
$\mu_x$	1.8360	2.0724	2.0705	2.0684	0.4178	0.2901	0.2936	0.2974
$\mu_y$	-2.0504	-2.6697	-2.6592	-2.6479	0.1035	0.0447	0.0461	0.0477
$\mu_z$	1.4148	1.7738	1.7679	1.7616	-0.1179	-0.2037	-0.2026	-0.2014
$\mu_t$	3.0946	3.8169	3.8057	3.7938	0.4463	0.3573	0.3597	0.3623
$\alpha_{xx}$	-89.00	-86.62	-86.66	-86.71	-100.53	-94.06	-94.17	-94.30
$\alpha_{yy}$	-87.85	-85.85	-85.89	-85.92	-119.92	-119.89	-119.89	-119.90
$\alpha_{zz}$	-79.56	-103.82	-103.82	-103.81	-122.07	-121.81	-121.81	-121.82
$\alpha_0$	85.47	-92.10	-92.12	-92.15	-114.17	-111.92	-111.96	-112.00
$\alpha$ (esu) * $10^{-24}$	-15.36	-13.65	-13.65	-13.66	-16.92	-16.59	-16.59	-16.60
$\beta_{xxx}$	92.28	107.75	107.58	107.39	-9.58	-16.90	-16.78	-16.65
$\beta_{xyy}$	-13.09	-12.79	-12.80	-12.81	37.07	40.21	40.17	40.12
$\beta_{xzz}$	4.27	5.59	5.58	5.56	12.83	13.95	13.93	13.91
$\beta_x$	83.46	100.55	100.35	100.14	40.31	37.25	37.32	37.39
$\beta_{yyy}$	-12.10	-14.02	-13.99	-13.96	36.18	35.02	35.04	35.07
$\beta_{xyy}$	-59.89	-71.00	-70.82	-70.64	27.57	29.39	29.38	29.36
$\beta_{yzz}$	-10.23	-10.97	-10.96	-10.94	1.06	0.23	0.25	0.26
$\beta_y$	-82.22	-95.99	-95.77	-95.54	64.81	64.64	64.66	64.69
$\beta_{zzz}$	-2.33	-0.38	-0.41	-0.44	-8.87	-8.48	-8.49	-8.50
$\beta_{xxx}$	27.19	33.36	33.26	33.17	-3.05	-4.43	-4.41	-4.38
$\beta_{yyz}$	-12.64	-12.88	-12.88	-12.88	4.76	5.43	5.42	5.40
$\beta_z$	12.22	20.09	19.97	19.84	-7.16	-7.47	-7.47	-7.47
$\beta_0$ (esu) * $10^{-33}$	117.791	140.456	140.149	139.831	76.661	74.976	75.333	75.093

Interestingly, Aspirin had the highest electronegativity (4.206 eV), showing its stronger ability to attract electrons within a molecule [47]. The chemical potential represents the average electron energy level and is directly related to electronegativity [48]. Notably, Aspirin had the most negative chemical potential (-4.206 eV), showing its electron-attracting nature. The electrophilicity values highlight the susceptibility of a molecule to act as an electrophile, while the nucleophilicity values represent its nucleophilic reactivity [49, 50]. Aspirin exhibited the highest electrophilicity and nucleophilicity values, showing its balanced reactivity as both an electron acceptor and donor. In terms of back-donation,

which quantifies electron transfer from the metal to ligands in coordination complexes, all compounds showed similar values, with Aspirin having the lowest magnitude. The electron transfer values representing the ability of a molecule to donate or receive electrons were higher for Aspirin and Diclofenac.

The total energy T.E in atomic units (a.u) provides insight into the stability of the compounds' electronic configurations [51, 52]. Among the investigated drugs, Diclofenac exhibited the lowest total energy, showing a relatively more stable electronic arrangement.

**Table 5.** Quantum chemical parameters for title compound.

Quantum chemical parameters	Paracetamol	Aspirin	naproxen	diclofenac
HOMO (eV)	-5.482	-6.927	-5.466	-5.553
LUMO (eV)	0.0081	-1.485	-1.052	-0.602
Ionization energy (eV)	5.482	6.927	5.466	5.553
Electron Affinity (eV)	-0.008	1.485	1.052	0.602
Energy gap (eV)	5.490	5.442	4.414	4.951
Hardness (eV)	2.745	2.721	2.207	2.476
Softness (eV) <sup>-1</sup>	0.182	0.184	0.227	0.202
Electronegativity (eV)	2.737	4.206	3.259	3.078
Chemical potential (eV)	-2.737	-4.206	-3.259	-3.078
Electrophilicity (eV)	1.364	3.251	2.406	1.913
Nucleophilicity (eV) <sup>-1</sup>	0.733	0.308	0.416	0.523
Back-donation (eV)	-0.686	-0.680	-0.552	-0.619
Electron transfer	0.997	1.546	1.477	1.243
Total energy T.E (a.u)	-515.499	-648.711	-767.633	-1665.745

## 2.7. Molecular Electrostatic Potential (MEP)

Fig. 7 depicts the Molecular Electrostatic Potential (MEP) color maps [53, 54], providing valuable insights into the electronic properties and charge distributions within the molecular structures of Paracetamol, Aspirin, Naproxen, and Diclofenac. The MEP color scheme, where red shows higher electronegativity and a negative charge, blue represents lower electronegativity and a positive charge, and green signifies neutrality, serves as a visual guide to discern the atoms' electronic behavior. Through this analysis, we can discern significant patterns among the compounds. Paracetamol exhibits a notable red region surrounding its oxygen atom,

showing its higher electronegativity compared to the adjacent blue region around the nitrogen atom. Similarly, aspirin displays red regions encircling both oxygen atoms and a blue region neighboring the carbon atom, revealing electronegativity disparities. Naproxen and Diclofenac also manifest red areas around their respective oxygen atoms and blue regions encircling carbon atoms, emphasizing charge separation because of electronegativity differences. These MEP discrepancies offer valuable insights into potential charge interactions and electron distributions within the molecular frameworks of these pharmaceutical compounds, enhancing our understanding of their electronic properties

and chemical reactivity.

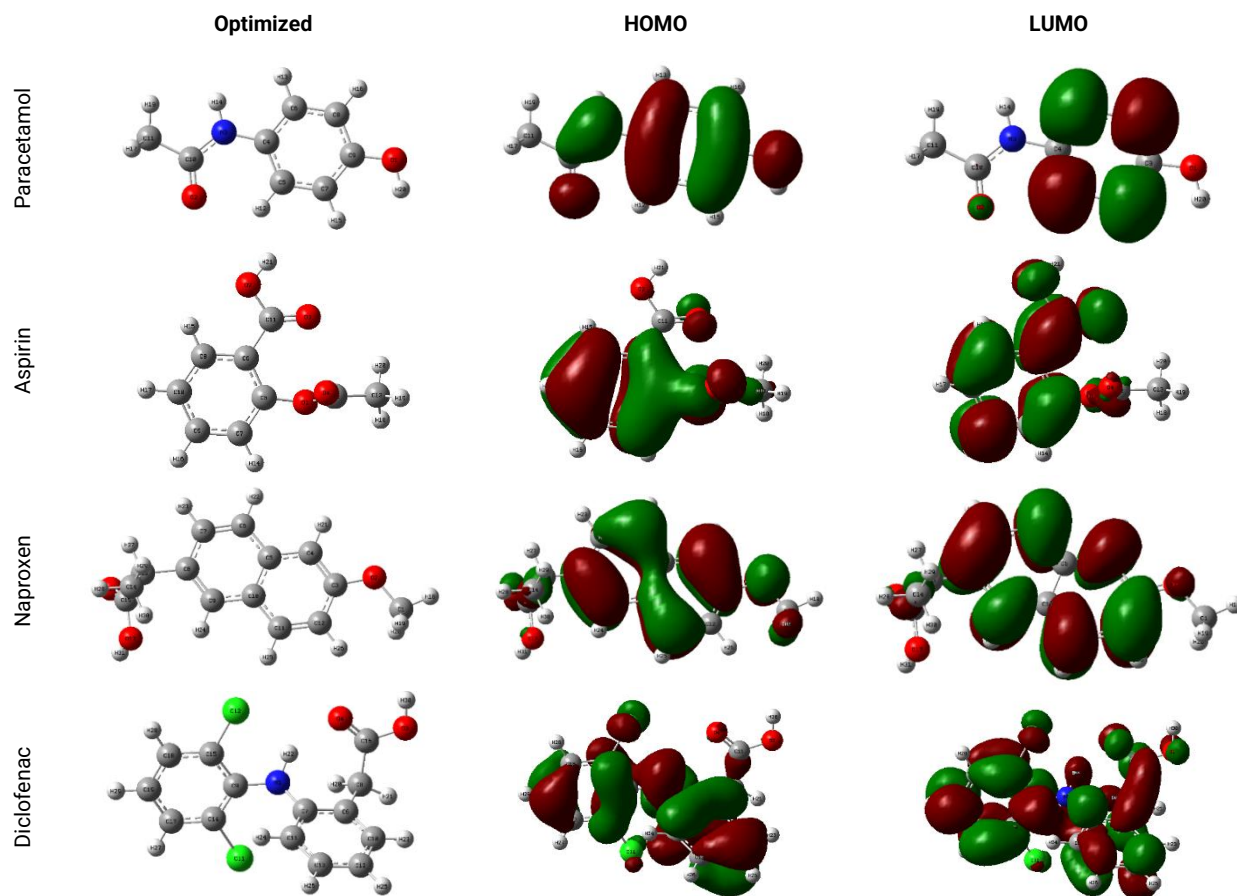


Fig. 6. optimized structures, HOMO, and LUMO energies for all compounds.

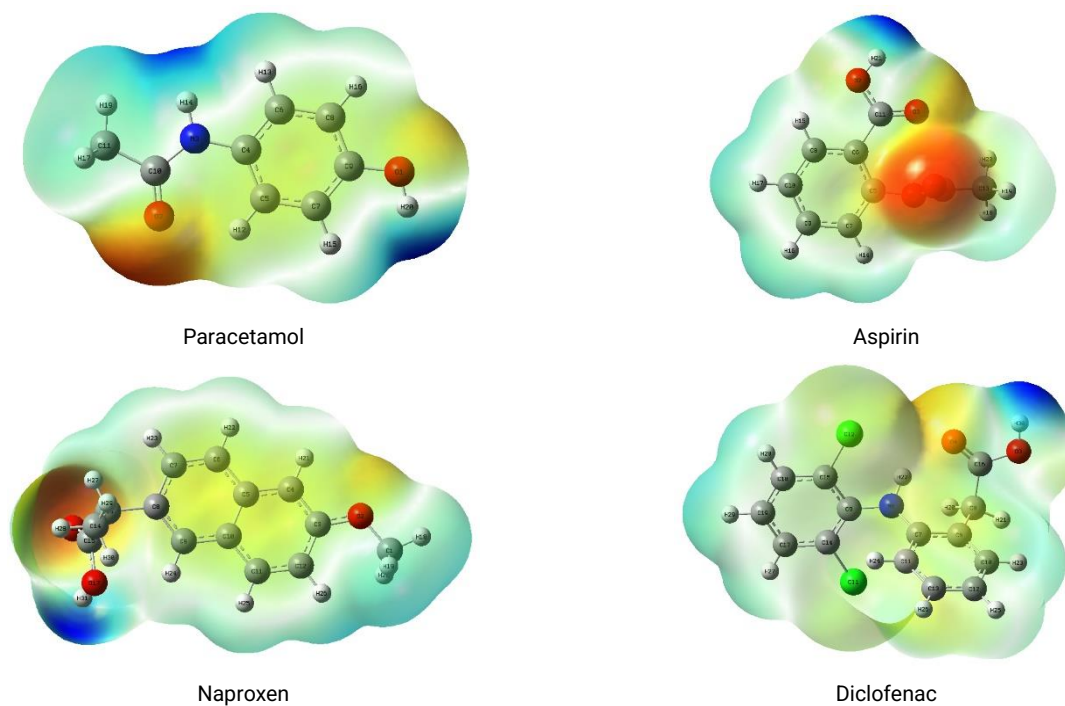


Fig. 7. Molecular Electrostatic Potential (MEP) for all compounds.

## 2.8. UV-Visible Spectra Analysis

Theoretical electronic absorption spectra provide

essential insights into the optical properties and potential applications of molecules [55, 56]. In this study, the UV-Vis



spectra of four pharmaceutical compounds, namely Paracetamol, Aspirin, Naproxen, and Diclofenac, were examined in various solvents to understand their electronic transitions and absorbance characteristics. Paracetamol exhibited absorption peaks in the gas phase at 4.7504 eV (261.00 nm) with an oscillator strength of 0.0331. The shift to solvent environments, such as water, DMSO, and methanol, resulted in slight variations in the absorption energy, wavelength, and oscillator strength. This shows that Paracetamol's electronic transitions are influenced by its surrounding media. Aspirin displayed absorption peaks at 4.6684 eV (265.58 nm) in the gas phase, with similar trends observed in different solvents. The relatively lower oscillator strength of Aspirin compared to Paracetamol might imply weaker electronic transitions and a lower probability of light absorption. Naproxen exhibited absorption peaks at 3.9889 eV (310.82 nm) in the gas phase, which shifted with varying solvents. Notably, Naproxen displayed the highest oscillator strength among the compounds, suggesting its relatively strong light-absorbing potential and efficient electronic transitions. Diclofenac's absorption peaks were observed at 4.3010 eV (288.27 nm) in the gas phase, showcasing differences in absorption behavior when exposed to distinct solvents see Table 6. The comparatively lower oscillator strength of Diclofenac indicates that it may have weaker absorbance characteristics compared to the other compounds. The oscillator strength (*f*) values indicate the probability of electronic transitions and are crucial in understanding the intensity of absorption bands. Higher *f* values suggest stronger transitions, which can be linked to the light absorption efficiency of the compounds. In pharmaceutical applications, this can influence photostability and drug efficacy, particularly for light-sensitive drugs.

**Table 6.** Theoretical electronic absorption spectra values for all compounds.

	Energy (eV)	Wavelength $\lambda$ (nm)	Oscillator strength ( <i>f</i> )
<b>Paracetamol</b>			
Gas phase	4.7504	261	0.0331
Water	4.7279	262.24	0.0441
DMSO	4.7243	262.44	0.0464
Methanol	4.7284	262.21	0.0439
<b>Aspirin</b>			
Gas phase	4.6684	265.58	0.0205
Water	4.6971	263.96	0.038
DMSO	4.6947	264.09	0.04
Methanol	4.6966	263.99	0.0375
<b>Naproxen</b>			
Gas phase	3.9889	310.82	0.0595
Water	3.9727	312.09	0.0793
DMSO	3.9677	312.48	0.0838
Methanol	3.9726	312.1	0.0791
<b>Diclofenac</b>			
Gas phase	4.301	288.27	0.019
Water	4.3279	286.48	0.0393
DMSO	4.3251	286.66	0.0555
Methanol	4.3256	286.63	0.0385

### 3. Material and Methods

#### 3.1. Computational details

The computational study involves Reduced Density Gradients (RDG) and Noncovalent Interactions (NCI) for characterizing weak intermolecular interactions. This study appears to focus on understanding interactions within molecules, particularly by utilizing RDG scatter plots, NCI

indices, and isosurfaces [57]. Hirschfeld surface technique and 2D fingerprint plots to analyze various types of intermolecular interactions within crystal structures. The findings provide insights into the distribution of electron density, presence of hydrogen bonding, and contributions of different interaction types to the Hirschfeld surface area [[30]][58]. Discussing a quantitative analysis of drug-likeness properties for Paracetamol, Aspirin, Naproxen, and Diclofenac. This analysis involves various descriptors to understand their pharmacological potential and guide rational drug design [33]. The study employs the B3LYP/6–31G (d, p) theoretical approach and NBO analysis to understand intramolecular and intermolecular hydrogen bonding, as well as the dispersion of  $\pi$  electrons within the molecule. The investigation also uses second-order energy calculations to estimate the stabilization energy and electron delocalization interactions between donor and acceptor NBOs. Computational analysis of non-linear optical properties of certain materials, including their dipole moments, polarizabilities, and initial hyper polarizabilities are investigating [39]. The quantum chemical parameters, including HOMO (Higher occupation molecular orbital) and LUMO (Lower occupation molecular orbital) provide insights into the reactivity, stability, and electronic behavior of the studied compounds. The detailed analysis helps to understand how these drugs interact chemically and how their electronic properties influence their behavior in various contexts [59]. Molecular Electrostatic Potential (MEP) color maps in providing insights into the electronic properties and charge distributions within the molecular structures [60]. The color scheme used in MEP maps helps visualize differences in electronegativity and charge within the molecules, leading to a better understanding of their electronic behavior and reactivity. The UV-Vis spectra in various solvents provide insights into the electronic transitions and absorbance characteristics of these pharmaceutical compounds. The oscillator strengths and absorption peaks highlight the differences in their light-absorbing potential and electronic behavior [61].

### 4. Conclusions

This study, through the integration of multiple advanced methodologies, has provided profound insights into the molecular, electronic, and optical properties of Paracetamol, Aspirin, Naproxen, and Diclofenac. The RDG and NCI analyses have illuminated the nature of their intermolecular interactions, revealing distinct patterns of hydrogen bonding,  $\pi \rightarrow \pi^*$  transitions, dispersion forces, and various attractive interactions. The NBO analysis further delved into the delicate balance between Lewis and non-Lewis orbitals, highlighting the significant role of electron delocalization in these compounds. Additionally, the quantum chemical parameter evaluation has offered a comparative framework for understanding their electronic characteristics. Aspirin's remarkable electron-accepting ability, demonstrated by its high ionization energy and electron affinity, contrasts with Paracetamol's electron-donating behavior, indicated by its lower HOMO energy. The MEP maps visually represented charge distribution, offering insights into their reactivity trends. The UV-Visible absorption spectra emphasized the compounds' optical properties, suggesting their potential for diverse applications. By combining various analytical techniques, including Aspirin's *miLogP* (1.43), Diclofenac's polar surface area (PSA) (49.33 Å<sup>2</sup>), and Paracetamol's molecular weight (151.16 g/mol), this study has woven a

comprehensive understanding of these compounds. These findings not only contribute to the advancement of drug design strategies but also expand the horizons of material science, providing valuable guidance for the development of optimized drugs and innovative materials. This research paves the way for the continued exploration and application of molecular properties, marking a new era of scientific discovery and innovation.

## Acknowledgments

We would like to thank the heads of the chemistry departments at Koya University for their support.

## Author Contributions

Yousif H. Azeez: Writing, original draft. Khdir A. Othman: Raining the molecule with DFT. Rebaz A. Omer: Writing: original draft and improving. Karzan A. Omer: Reviewing and improving the original draft. Aryan F. Qader: Validation, Writing, Review, and Editing.

## References

- [1] Liu, F.; Ma, C.; McClements, D. J.; Gao, Y. *Food Hydrocolloids* **2017**, 63, 625. [\[Crossref\]](#)
- [2] Saleh, G.; Gatti, C.; Presti, L. L. *Comput. Theor. Chem.* **2012**, 998, 148. [\[Crossref\]](#)
- [3] Priscilla, J.; Dhas, D. A.; Joe, I. H.; Balachandran, S. *Chem. Phys.* **2020**, 536, 110827. [\[Crossref\]](#)
- [4] Boto, R. A.; Piquemal, J.-P.; Contreras-García, J. *Theor. Chem. Acc.* **2017**, 136, 1. [\[Crossref\]](#)
- [5] Kourat, O.; Djafri, A.; Benhalima, N.; Megrouss, Y.; Belkafouf, N. E. H.; Rahmani, R.; Daran, J.-C.; Djafri, A.; Chouaih, A. *J. Mol. Struct.* **2020**, 1222, 128952. [\[Crossref\]](#)
- [6] Isik, I. B.; Tekin, N.; Sagdinc, S. G. *J. Mol. Struct.* **2022**, 1250, 131861. [\[Crossref\]](#)
- [7] Nithya, S.; Aranganayagam, K.; Shekar, B. Hirshfeld surface analysis of 2-amino-6-methyl pyridinium barbiturate tetrahydrate organic single crystal, AIP Conference Proceedings, AIP Publishing, 2022. [\[Crossref\]](#)
- [8] Jarrahpour, A.; Fathi, J.; Mimouni, M.; Hadda, T. B.; Sheikh, J.; Chohan, Z.; Parvez, A. *Med. Chem. Res.* **2012**, 21, 1984. [\[Crossref\]](#)
- [9] Mabkhot, Y. N.; Alatibi, F.; El-Sayed, N. N. E.; Al-Showiman, S.; Kheder, N. A.; Wadood, A.; Rauf, A.; Bawazeer, S.; Hadda, T. B. *Molecules* **2016**, 21, 222. [\[Crossref\]](#)
- [10] Prasad, A. A.; Muthu, K.; Meenatchi, V.; Rajasekar, M.; Agilandeshwari, R.; Meena, K.; Manonmoni, J. V.; Meenakshisundaram, S. *Spectrochim. Acta, Part A* **2015**, 140, 311. [\[Crossref\]](#)
- [11] Gangadharan, R.; Sampath Krishnan, S. *Acta Phys. Pol. A* **2014**, 125, 18. [\[Crossref\]](#)
- [12] Atlam, F. M.; Awad, M. K.; El-Bastawissy, E. A. *J. Mol. Struct.* **2014**, 1075, 311. [\[Crossref\]](#)
- [13] Syrovaya, A.; Chalenko, N.; Tishakova, T.; Kozub, S.; Levashova, O. *Der Pharma Chemica* **2017**, 9, 11.
- [14] Chekman, I.; Syrovaya, A.; Levashova, O.; Tishakova, T.; Kozub, S.; Chalenko, N. *Sci. Eur.* **2019**, 38, 32.
- [15] Ahmed, L.; Bulut, N.; Kaugili, O.; Rebaz, O. *J. Phys. Chem. Funct. Mater.* **2023**, 6, 34. [\[Crossref\]](#)
- [16] Rasul, H. H.; Mamad, D. M.; Azeez, Y. H.; Omer, R. A.; Omer, K. A. *Comput. Theor. Chem.* **2023**, 114177. [\[Crossref\]](#)
- [17] Parlak, A. E.; Omar, R. A.; Koparir, P.; Salih, M. I. *Arabian J. Chem.* **2022**, 15, 104088. [\[Crossref\]](#)
- [18] Koparir, P.; Omar, R. A.; Sarac, K.; Ahmed, L. O.; Karatepe, A.; Taskin-Tok, T.; Safin, D. A. *Polycyclic Aromat. Compd.* **2022**, 1. [\[Crossref\]](#)
- [19] Kwok, C. S.; Loke, Y. K. *Pharmaceuticals* **2010**, 3, 1491. [\[Crossref\]](#)
- [20] Prescott, L. F. *Am. J. Ther.* **2000**, 7, 143.
- [21] Kaduševičius, E. *Int. J. Mol. Sci.* **2021**, 22, 6637. [\[Crossref\]](#)
- [22] Pandey, S. K.; Yadav, S.; Goel, Y.; Temre, M. K.; Singh, V. K.; Singh, S. M. *J. Theor. Biol.* **2019**, 465, 117. [\[Crossref\]](#)
- [23] Rebaz, O.; Ahmed, L.; Koparir, P.; Jwameer, H. *El-Cezeri* **2022**, 9, 740. [\[Crossref\]](#)
- [24] Domingo, L. R.; Aurell, M. J.; Pérez, P.; Contreras, R. *Tetrahedron* **2002**, 58, 4417. [\[Crossref\]](#)
- [25] Asath, R. M.; Rekha, T.; Premkumar, S.; Mathavan, T.; Benial, A. M. F. *J. Mol. Struct.* **2016**, 1125, 633. [\[Crossref\]](#)
- [26] Boukabcha, N.; Benmohammed, A.; Belhachemi, M. H. M.; Goudjil, M.; Yahiaoui, S.; Megrouss, Y.; Djafri, A.; Khelloul, N.; Benyehlou, Z. D.; Djafri, A. *J. Mol. Struct.* **2023**, 1285, 135492. [\[Crossref\]](#)
- [27] Humphrey, W.; Dalke, A.; Schulten, K. *J. Mol. Graphics* **1996**, 14, 33. [\[Crossref\]](#)
- [28] Saidj, M.; Djafri, A.; Rahmani, R.; Belkafouf, N. E. H.; Boukabcha, N.; Djafri, A.; Chouaih, A. *Polycyclic Aromat. Compd.* **2023**, 43, 2152. [\[Crossref\]](#)
- [29] Guerroudj, A. R.; Boukabcha, N.; Benmohammed, A.; Dege, N.; Belkafouf, N. E. H.; Khelloul, N.; Djafri, A.; Chouaih, A. C. *J. Mol. Struct.* **2021**, 1240, 130589. [\[Crossref\]](#)
- [30] Benyahlou, Z. D.; Baara, F. T.; Yahiaoui, S.; Megrouss, Y.; Boukabcha, N.; Djafri, A.; Chouaih, A.; Hatzidimitriou, A. *J. Mol. Struct.* **2023**, 1277, 134781. [\[Crossref\]](#)
- [31] Turner, M.; McKinnon, J.; Wolff, S.; Grimwood, D.; Spackman, P.; Jayatilaka, D.; Spackman, M. CrystalExplorer17, The University of Western Australia Australia, 2017.
- [32] Mansour, A.; Souheyla, C.; Youcef, M.; Nourdine, B.; Amel, D.; Roufieda, G. A.; Nouredine, M. A.; Abdelkader, C. *J. Mol. Struct.* **2022**, 1261, 132887. [\[Crossref\]](#)
- [33] Ursu, O.; Rayan, A.; Goldblum, A.; Oprea, T. I. *Wiley Interdiscip. Rev.:Comput. Mol. Sci.* **2011**, 1, 760. [\[Crossref\]](#)
- [34] Desai, N.; Kotadiya, G.; Trivedi, A. *Bioorg. Med. Chem. Lett.* **2014**, 24, 3126. [\[Crossref\]](#)
- [35] Ranjith, P.; Ignatious, A.; Panicker, C. Y.; Sureshkumar, B.; Armakovic, S.; Armakovic, S. J.; Van Alsenoy, C.; Anto, P. *J. Mol. Struct.* **2022**, 1264, 133315. [\[Crossref\]](#)
- [36] Sumathi, D.; Thanikachalam, V.; Bharanidharan, S.;

- Saleem, H.; Babu, N.R. *International J. Scient. Res.* **2016**, 5, 694. [\[Link\]](#)
- [37] Abbaz, T.; Bendjeddou, A.; Villemin, D. *International J. Adv. Chem.* **2017**, 6, 18. [\[Crossref\]](#)
- [38] Villemin, D.; Abbaz, T.; Bendjeddou, A. *Pharm. Biol. Eval.* **2018**, 5. [\[Crossref\]](#)
- [39] Abbaz, T.; Bendjeddou, A.; Villemin, D. **2018**, 6, 114. [\[Crossref\]](#)
- [40] Obot, I.; Macdonald, D.; Gasem, Z. *Corrosion Science* **2015**, 99, 1. [\[Crossref\]](#)
- [41] Khan, M. U.; Khalid, M.; Asim, S.; Momina; Hussain, R.; Mahmood, K.; Iqbal, J.; Akhtar, M. N.; Hussain, A.; Imran, M. *Front. Mat.* **2021**, 8, 719971. [\[Crossref\]](#)
- [42] Al-Shamiri, H. A.; Sakr, M. E.; Abdel-Latif, S. A.; Negm, N. A.; Abou Kana, M. T.; El-Daly, S. A.; Elwahy, A. H. *Sci. Rep.* **2022**, 12, 19937. [\[Crossref\]](#)
- [43] Fedorov, D. G.; Kitaura, K. J. *Phys. Chem. A* **2007**, 111, 6904. [\[Crossref\]](#)
- [44] Tariq, A.; Nazir, S.; Arshad, A. W.; Nawaz, F.; Ayub, K.; Iqbal, J. *RSC advances* **2019**, 9, 24325. [\[Crossref\]](#)
- [45] Fulton, A.; Lyons, L. E. *Aust. J. Chem.* **1968**, 21, 873. [\[Crossref\]](#)
- [46] Chaudhary, M. K.; Srivastava, A.; Singh, K. K.; Tandon, P.; Joshi, B. D. *Comput. Theor. Chem.* **2020**, 1191, 113031. [\[Crossref\]](#)
- [47] Bultinck, P.; Langenaeker, W.; Carbó-Dorca, R.; Tollenaere, J. P. J. *Chem. Inf. Comput. Sci.* **2003**, 43, 422. [\[Crossref\]](#)
- [48] Allen, L. C. *Int. J. Quantum Chem.* **1994**, 49, 253. [\[Crossref\]](#)
- [49] Mayr, H.; Patz, M. *Angew. Chem., Int. Ed. Engl.* **1994**, 33, 938. [\[Crossref\]](#)
- [50] Kiyooka, S.-i.; Kaneno, D.; Fujiyama, R. *Tetrahedron Lett.* **2013**, 54, 339. [\[Crossref\]](#)
- [51] Park, H.; Millis, A. J.; Marianetti, C. A. *Phys. Rev. B* **2014**, 89, 245133. [\[Crossref\]](#)
- [52] Lin, L.; Lu, J.; Ying, L.; Weinan, E. J. *Comput. Phys.* **2012**, 231, 2140. [\[Crossref\]](#)
- [53] Murray, J. S.; Politzer, P. *Wiley Interdiscip. Rev.:Comput. Mol. Sci.* **2011**, 1, 153. [\[Crossref\]](#)
- [54] Pullman, A.; Pullman, B. Q. *Rev. Biophys.* **1981**, 14, 289. [\[Crossref\]](#)
- [55] Uddin, M. A.; Sutoanu, B. H.; Rub, M. A.; Mahbub, S.; Alotaibi, M. M.; Asiri, A. M.; Rana, S.; Hoque, M. A.; Kabir, M. *Korean J. Chem. Eng.* **2022**, 1. [\[Crossref\]](#)
- [56] Muhammad, S.; Shkir, M.; AlFaify, S.; Irfan, A.; Al-Sehemi, A. G. *RSC Advances* **2015**, 5, 53988. [\[Crossref\]](#)
- [57] Premkumar, S.; Rekha, T.; Asath, R. M.; Mathavan, T.; Benial, A. M. F. *Eur. J. Pharm. Sci.* **2016**, 82, 115. [\[Crossref\]](#)
- [58] Al-Harbi, S. A.; Abdulrahman, A. O.; Zamzami, M. A.; Khan, M. I. *Front. Nutrition* **2021**, 8, 647582. [\[Crossref\]](#)
- [59] Rebaz, O.; Koparir, P.; Qader, I. N.; Ahmed, L. *Cumhuriyet Sci. J.* **2021**, 42, 576. [\[Crossref\]](#)
- [60] Rebaz, O.; Ahmed, L.; Jwameer, H.; Koparir, P. *El-Cezeri* **2022**, 9, 760. [\[Crossref\]](#)
- [61] Omer, R. A.; Koparir, P.; Ahmed, L. O. *Journal of Bio-and Tribo-Corrosion* **2022**, 8, 28. [\[Crossref\]](#)

## How to cite this article

Azeez, Y. H.; Omer, R. A.; Othman, K. A.; Omar, K. A.; Qader, A. F. *Orbital: Electronic J. Chem.* **2025**, 17, 50. DOI: <http://dx.doi.org/10.17807/orbital.v17i1.19889>